EDINBURGH INSTRUMENTS

50 YEARS 1971-2021

PRECISION RAMAN

Best-in-class Raman microscopes
for research and analytical requirements backed with world-class customer support and service.

edinst.com

Research Article

Journal of RAMAN SPECTROSCOPY

Received: 25 April 2009 Accepted: 1 July 2009 Published online in Wiley Interscience: 8 September 2009

(www.interscience.wiley.com) DOI 10.1002/jrs.2408

Molecular structure, vibrational spectroscopic, first-order hyperpolarizability and HOMO, LUMO studies of 3-hydroxy-2-naphthoic acid hydrazide

J. Karpagam,[a] N. Sundaraganesan,[a]* S. Sebastian,[a] S. Manoharan[b] and M. Kurt[c]

The Fourier-transform infrared spectrum of 3-hydroxy-2-naphthoic acid hydrazide (3H2NAH) was recorded in the region 4000–400 cm^{-1}. The Fourier-transform Raman spectrum of 3H2NAH was also recorded in the region 3500–10 cm^{-1}. Quantum chemical calculations of energies, geometrical structure and vibrational wavenumbers of 3H2NAH were carried out by density functional theory (DFT/B3LYP) method with 6-31G(d,p) as basis set. The difference between the observed and scaled wavenumber values of most of the fundamentals is very small. The values of the electric dipole moment (μ) and the first-order hyperpolarizability (β) of the investigated molecule were computed using *ab initio* quantum mechanical calculations. The UV spectrum was measured in ethanol solution. The calculation results also show that the 3H2NAH molecule might have microscopic nonlinear optical (NLO) behavior with non-zero values. A detailed interpretation of the infrared and Raman spectra of 3H2NAH is also reported based on total energy distribution (TED). The calculated HOMO and LUMO energies shows that charge transfer occur within the molecule. The theoretical FT-IR and FT-Raman spectra for the title molecule have also been constructed.

Supporting information may be found in the online version of this article.

Keywords: vibrational spectra; DFT; first-order hyperpolarizability; HOMO; LUMO; TED; 3-hydroxy-2-naphthoic acid hydrazide

Introduction

Tuberculosis (TB) is one of the leading causes of death due to a single infectious organism in the world. As per survey reported by Global Alliances, Geneva, there are 8–10 million new active cases of TB and approximately 3 million deaths each year.[1–4] Treatment of TB infection that has been caused by multi-drug-resistant (MDR), *Mycobacterium tuberculosis* has become major concern the world over. The term MDR TB is used to describe strains that are resistant to one or more anti-tuberculosis drugs.[5–7] The hydrazide group is an oxidatively cleavable traceless linker for solid-phase chemistry. This linker technology was used to develop a multi-step solid-phase synthesis of an antibiotic that is active against *M. tuberculosis*.[8]

Bioactivities of various acyl hydrazones are well reported in literature.[9,10] They are synthesized by simply refluxing acid hydrazide with various carbonyl compounds in methanol or ethanol. Due to the simple reaction conditions, diversified chemical libraries may be constructed for discovering potential bioactive molecules. The resulting double bond between C and N of the hydrazones contributes to the formation of geometrical isomers (*syn* and *anti*). Geometrical isomerism may have some important role in the bioactivity of the acyl hydrazones, and hence their studies are very crucial to develop synthetic methods for selective synthesis of a particular isomer.

The infrared absorption spectra of hydrazides and monoacid hydrazides have been reported by Mashima.[11] A novel tetranuclear copper(II) cluster containing twisted hydrazide bridges has been synthesized, and X-ray crystal structure and magnetic properties of tetrakis[*N*,*N*′-imidopicolinyloxamylhydrazine) copper(II)] tetranitrate octahydrate have been carried out by Koningsbruggen *et al*.[12] Samdal and Møllendal[13] studied formichydrazide (formylhydrazine) by microwave spectroscopy, and quantum chemical *ab initio* and density functional theory (DFT) calculations were carried out at various levels of theory. Both the *ab initio* and the DFT calculations predict that two stable forms exist for this compound.

The hydrazides of (tetrazol-1-yl)-and(tetrazol-2-yl) acetic acids and their deuterated analogs were investigated by means of IR spectroscopy by Sinditskii *et al*.[14] Only the synthesis, structure elucidation and antimicrobial activity of 3-hydroxy-2-naphthoic acid hydrazide (3H2NAH) derivatives have been carried out by Dogan *et al*.[15] To our knowledge, the vibrational spectra and the theoretical calculations of 3H2NAH have not been

* *Correspondence to: N. Sundaraganesan, Department of Physics (Engg.), Annamalai University, Annamalai Nagar, Tamil Nadu 608002, India. E-mail: sundaraganesan_n2003@yahoo.co.in*

a *Department of Physics (Engg.), Annamalai University, Annamalai Nagar, Tamil Nadu 608002, India*

b *Department of Biochemistry and Biotechnology, Annamalai University, Annamalai Nagar, Tamil Nadu 608002, India*

c *Ahi Evran Üniversitesi Fen Edebiyat Fakültesi Fizik Bölümü, Aşıkpaşa Kampusü 40100 Kirşehir-Turkiye, Turkey*

reported except in our work. FT-IR and NIR-FT-Raman spectroscopy combined with quantum chemical computations has been recently used as an effective tool in the vibrational analysis of drug molecules,[16] biological compounds[17] and natural products,[18] since fluorescence-free Raman spectra and the computed results can help unambiguous identification of vibrational modes as well as the bonding and structural features of complex organic molecular systems. IR, Raman and UV spectroscopic studies along with HOMO, LUMO and hyperpolarizability analysis have been used to elucidate information regarding charge transfer within the molecule. The present work deals with DFT computations and vibrational spectral analysis of 3H2NAH on the basis of the calculated total energy distribution (TED).

Experimental

The compound 3H2NAH in the solid form was purchased from the Sigma–Aldrich Chemical Company (USA) with a stated purity of greater than 98% and was used as such without further purification. The FT-Raman spectra of 3H2NAH were recorded using the1064 nm line of a Nd : YAG laser as excitation wavelength in the region 10–3500 cm^{-1} on a Brucker model IFS 66 V spectrophotometer equipped with an FRA 106 FT-Raman module accessory. The FT-IR spectrum of this compound was recorded in the region 400–4000 cm^{-1} on an IFS 66V spectrophotometer using the KBr pellet technique. The spectra were recorded at room temperature, with a scanning speed of 10 cm^{-1} per minute and at the spectral resolution of 2.0 cm^{-1}. The observed experimental FT-IR and FT-Raman spectra along with theoretical spectra are shown in Figs 1 and 2. The ultraviolet absorption spectra of 3H2NAH were examined in the range 200–800 nm using a Shimadzu UV-2401PC, UV–Vis recording spectrometer. The UV pattern is taken from a 10^{-5} molar solution of 3H2NAH, dissolved in ethanol as shown in Fig. 3. The spectral measurements were carried out at Sree Chitra Tirunal Institute for Medical Sciences and Technology, Poojappura, Thiruvanathapuram, Kerala, India.

Computational Details

For meeting the requirements of both accuracy and computing economy, theoretical methods and basis sets should be considered. DFT has proved to be extremely useful in treating electronic structure of molecules. The basis set 6-31G(d,p) was used as a effective and economical level to study fairly large organic

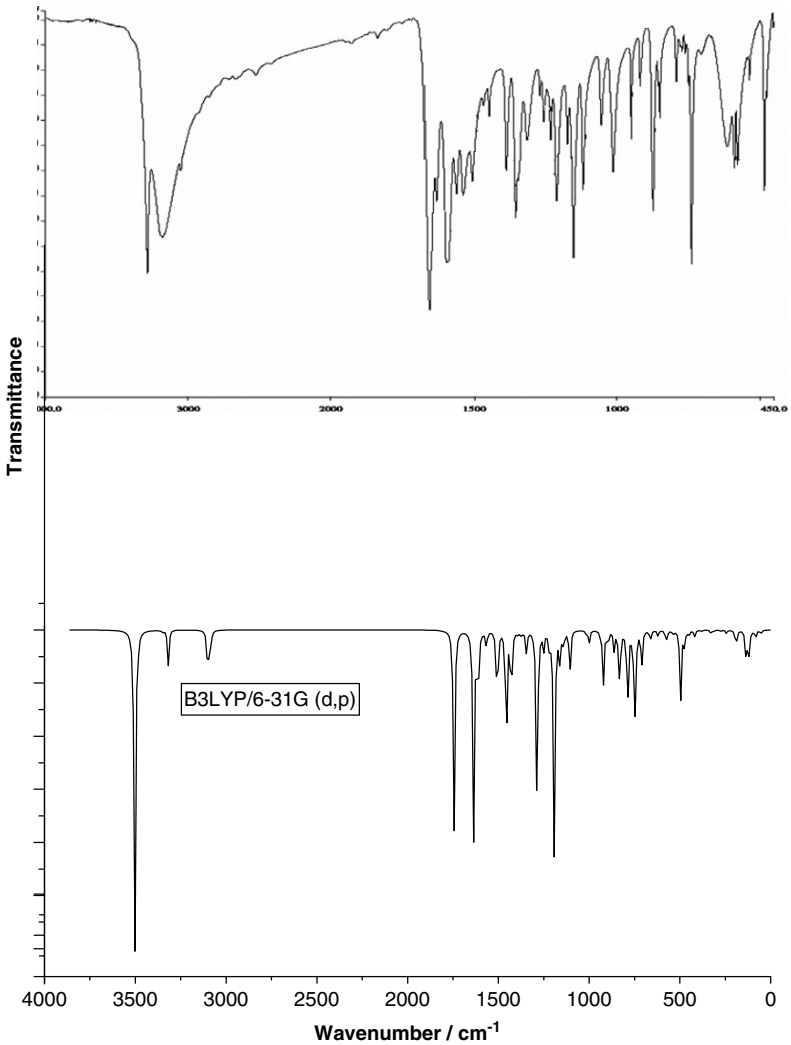

Figure 1. Comparison of the observed and computed FT-IR Spectra of 3- hydroxy-2-naphthoic acid hydrazide.

Journal of RAMAN SPECTROSCOPY

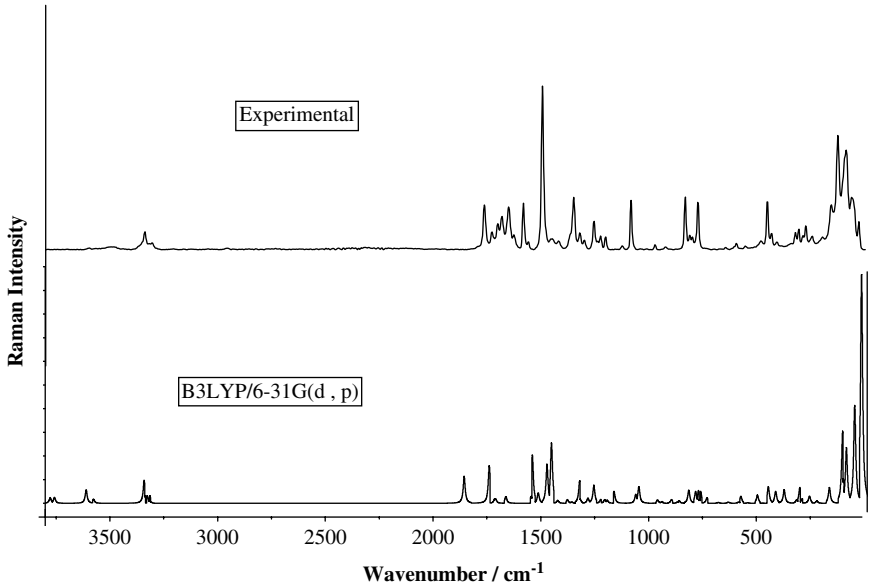

Figure 2. Comparison of the observed and computed FT-Raman Spectra of 3-hydroxy-2-naphthoic acid hydrazide.

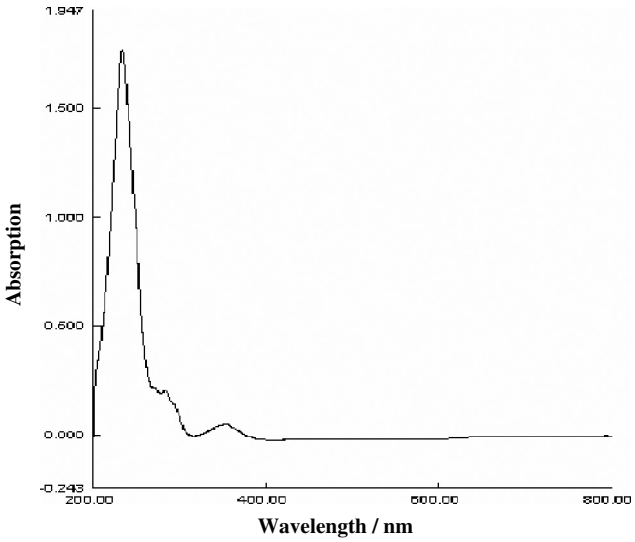

Figure 3. UV-visible spectrum of 3-hydroxy-2-naphthoic acid hydrazide.

molecules. Based on these points, the density functional three-parameter hybrid model (DFT/B3LYP) at the 6-31G(d,p) basis set level along with HF method was adopted to calculate the properties of the studied molecule in this work. All the calculations were performed using the Gaussion 03W program package[19] with the default convergence criteria without any constraint on the geometry.[20] Geometries of the model 3H2NAH were first optimized with full relaxation on the potential energy surfaces at HF/6-31G(d,p) level, and the resultant geometries were used as inputs for further calculations at the DFT(B3LYP) level. Polarization functions were added for the better treatment of the hydroxyl, amino and hydrizide groups. The optimized structural parameters were used in the vibrational wavenumber calculation at DFT level to characterize all stationary points as minima. The total energy distribution (TED) was calculated by using the scaled quantum mechanics (SQM) program,[21,22] and the fundamental vibrational modes were characterized by their TED.

Prediction of Raman intensities and hyperpolarizability

The Raman activities (S_i) calculated with Gaussian 03 program[19] converted to relative Raman intensities (I_i) using the following relationship derived from the intensity theory of Raman scattering:[23,24]

$$I_i = \frac{f(\nu_o - \nu_i)^4 S_i}{\nu_i[1 - \exp(-hc\nu_i/kt)]}$$

where ν_o is the exciting wavenumber in cm^{-1}, ν_i the vibrational wavenumber of the ith normal mode, h, c and k are fundamental constants and f is a suitably chosen common normalization factor for all peak intensities. For simulation, the calculated FT-Raman spectra were plotted using a pure Lorentizian band shape with a bandwidth of full width and half-maximum (FWHM) of 10 cm^{-1} as shown in Fig. 2. In the FT-IR spectra, the theoretically simulated spectra are more regular than the experimental ones, because many vibrations presenting in condensed phase lead to strong perturbation of infrared intensities of many other modes.

The first hyperpolarizability (β_0) of this novel molecular system and the related properties (β, $\alpha 0$ and $\Delta\alpha$) of 3H2NAH were calculated using the HF/6-31G(d,p) basis set, based on the finite-field approach. In the presence of an applied electric field, the energy of a system is a function of the electric field. The first hyperpolarizability is a third-rank tensor that can be described by a $3 \times 3 \times 3$ matrix. The 27 components of the 3D matrix can be reduced to 10 components due to the Kleinman symmetry.[25] It can be given in the lower tetrahedral format. It is obvious that the lower part of the $3 \times 3 \times 3$ matrixes is tetrahedral. The components of β are defined as the coefficients in the Taylor series expansion of the energy in the external electric field. When the external electric field is weak and homogeneous, this expansion becomes:

$$E = E^0 - \mu_\alpha F_\alpha - 1/2\alpha_{\alpha\beta}F_\alpha F_\beta - 1/6\beta_{\alpha\beta\gamma}F_\alpha F_\beta F_\gamma + \ldots$$

where E^0 is the energy of the unperturbed molecules, F_α the field at the origin and μ_α, $\alpha_{\alpha\beta}$ and $\beta_{\alpha\beta\gamma}$ are the components of dipole moment, polarizability and the first hyperpolarizabilities,

respectively. The total static dipole moment μ, the mean polarizability α_0, the anisotropy of the polarizability $\Delta\alpha$ and the mean first hyperpolarizability β_0, using the *x*, *y*, *z* components they are defined as follows:

$$\mu = (\mu^2{}_x + \mu^2{}_y + \mu^2{}_z)^{1/2}$$

$$\alpha_0 = \frac{\alpha_{xx} + \alpha_{yy} + \alpha_{zz}}{3}$$

$$\alpha = 2^{-1/2}[(\alpha_{xx} - \alpha_{yy})^2 + (\alpha_{yy} - \alpha_{zz})^2 + (\alpha_{zz} - \alpha_{xx})^2 + 6\alpha^2 xx]^{1/2}$$

$$\beta 0 = (\beta^2{}_x + \beta^2{}_y + \beta^2{}_z)^{1/2}$$

and

$$\beta_x = \beta_{xxx} + \beta_{xyy} + \beta_{xzz}$$
$$\beta_y = \beta_{yyy} + \beta_{xxy} + \beta_{yzz}$$
$$\beta_z = \beta_{zzz} + \beta_{xxz} + \beta_{yyz}$$

The HF/6-31G (d,p) calculated first hyperpolarizability of 3H2NAH is 0.0245×10^{-30} esu, and is shown in Table S1 (Supporting Information). The total molecular dipole moment (μ) and mean first hyperpolarizability (β) *are* given directly here, 4.4832 debye and 0.0245×10^{-30} esu respectively shown in Table S1 (Supporting Information). The total dipole moment of title compound is approximately 3 times greater than those of urea, and first hyperpolarizability of title molecule is 15 times smaller than those of urea (μ and β of urea are 1.3732 debye and 0.3728×10^{-30} esu obtained by HF/6-31G(d,p) method).

Results and Discussions

Geometric structure

The optimized structure parameters of 3H2NAH calculated by DFT (B3LYP) level with the 6-31G(d,p) basis set are listed in Table S2 (Supporting Information), in accordance with the atom numbering scheme in Fig. 4. All the geometries determined belong to a true minimum proven by real wavenumbers in the vibrational analysis as seen from Table 1. To the best of our knowledge, exact experimental data on the geometrical parameters of 3H2NAH are not available in the literature. Therefore, we could not compare the calculation results given in Table S2 (Supporting Information) with the experimental data. Therefore, the crystal data of a closely related molecule such as 6-methoxy-2-naphthaldehyde[26] is compared with that of the title molecule. As seen from Table S2 (Supporting Information), most of the optimized bond lengths are slightly longer than the experimental values and the bond angles are slightly different from the experimental ones, because the molecular states are different during experimental and theoretical processes. One isolated molecule is considered in gas phase in theoretical calculation, whereas many packed molecules are treated in condensed phase during the experimental measurement. The naphthalene ring is planar, and also the O atom of the hydroxyl group and C atom of carbonyl groups are lying approximately in the plane as evident from the torsional angles C11–C14–C15–O17 = 177.7° and C4–C11–C14–C19 = 179.8°, respectively, by B3LYP/6-31G(d,p) method. The variation in torsional angles C15–C14–C19–O20 = −153.2° and C14–C15–O17–H18 = 6.6° is due to charge delocalization. The hydroxyl group makes an dihedral of 6.67° with the plane defined by the atoms C1, C2, C3, C4, C5, C6, C10, C11, C14 and C15, while the carbonyl group makes an angle of 24.49° with the plane defined by the atoms C1, C2, C3, C4, C5, C6, C10, C11 and C15, indicating steric hindrance. These values are comparable with reported value available in the literature.[26] For the first ring, the C–C bond lengths vary from 1.376 to 1.435 Å by B3LYP method, and for the second ring, the C–C bond length varies from 1.385 to 1.435Å by same method. The second benzene ring appears to be a little distorted because of

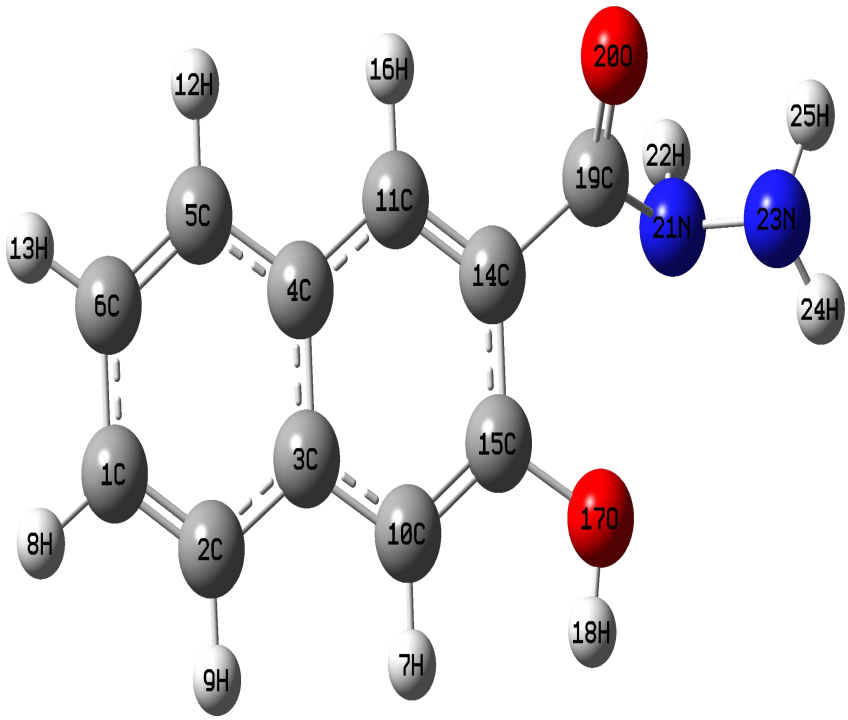

Figure 4. Atom numbering scheme adopted in this study for 3-hydorxy-2- naphthoic acid hydrazide.

Table 1. Vibrational wavenumbers obtained for 3H2NAH at B3LYP/6-31G(d,p) method [harmonic wavenumber (in cm^{-1}), IR_{int} (km mol^{-1}), S_{act}($Å^4$/amu)]

	Experimental (cm^{-1})		Theoretical wavenumber (cm^{-1})				
Mode nos.	FT-IR	FT-Raman	B3LYP unscaled	B3LYP scaled	IR_{int}	S_{act}	Characterization of normal modes with TED
1		67w	53	51	3.49	3.43	$\Gamma_{CCCC}(10) + \Gamma_{OCCC}(15) + \Gamma_{NCCC}(40) + \Gamma_{HNCC}(9) + \Gamma_{NNCC}(9)$
2		98m	83	80	7.57	3.76	$\Gamma_{NCCC}(9) + \Gamma_{OCCC}(30) + \Gamma_{CCCC}(31)$
3			119	115	21.80	3.50	$\Gamma_{HNNC}(27)$
4		120s	134	128	3.98	2.58	$\delta_{CCC}(28)\ \Gamma_{NNCC}(16)$
5		155vs	136	131	33.52	6.00	$\Gamma_{CCCC}(12)\ \Gamma_{OCCC}(11)\ \Gamma_{HNNC}(23)$
6		183m	194	187	17.46	2.18	$\delta_{CCC}(11)\ \Gamma_{HNNC}(12)$
7			250	240	2.98	0.49	$\delta_{CCC}(10)\ \delta_{NCN}(11)\ \Gamma_{NNCC}(16)$
8		262m	282	271	1.20	1.79	$\delta_{CCN}(10)\ \Gamma_{OCCC}(16)$
9		289m	314	302	0.22	1.35	$\delta_{CCC}(11)\ \Gamma_{OCCC}(12)$
10		319m	325	312	1.55	4.77	$\nu_{CC}(10)\ \delta_{CCC}(42)$
11		322m	338	325	2.68	1.18	$\delta_{CCC}(37)\ \delta_{NNC}(18)\ \Gamma_{HNNH}(11)$
12			393	378	1.32	5.29	$\delta_{OCC}(26)\ \delta_{CCN}(17)$
13			431	414	6.01	5.23	$\delta_{CCC}(13) + \Gamma_{CCCC}(11)$
14		432m	463	445	5.33	8.27	$\nu_{CC}(14)\ \delta_{CCC}(12)$
15		450s	489	469	14.88	0.15	$\Gamma_{CCCC}(55) + \Gamma_{HCCC}(13)$
16	483s		511	491	68.30	4.44	$\Gamma_{HOCC}(35) + \Gamma_{HNNH}(21)$
17	536w		553	532	4.17	0.37	$\Gamma_{CCCC}(53)$
18			583	561	2.15	4.58	$\delta_{CCC}(36)\ \delta_{OCC}(20)$
19	578w	579w	593	570	11.13	0.90	$\nu_{CC}(20)\ \delta_{CCC}(53)$
20	618m		639	614	5.38	0.88	$\delta_{CCC}\ (57)\ \delta_{CCH}(11)$
21			683	656	9.53	0.74	$\Gamma_{CCCH}(18) + \Gamma_{OCCC}(19)$
22	703w		733	704	40.72	4.98	$\nu_{CC}(10)\ \delta_{CCC}(19)$
23			761	731	2.65	10.97	$\Gamma_{HCCC}(35)$
24			765	735	1.10	3.52	$\Gamma_{CCCC}(47) + \Gamma_{HCCC}(25)$
25	738vs	740ms	770	740	75.61	12.26	$\Gamma_{HCCC}(37)$
26	772w	774w	783	752	18.69	11.23	$\nu_{NC}(12) + \delta_{OCN}(11)\ \Gamma_{OCCC}(10)$
27	792ms	793ms	813	781	80.04	13.53	$\nu_{CC}(33) + \Gamma_{HOCC}(17)$
28			856	822	45.60	2.88	$\delta_{NNH}(13)\ \Gamma_{CNNH}(10) + \Gamma_{HNNH}(17)$
29			863	829	21.08	1.40	$\Gamma_{CCCH}(50)$
30	850m		889	854	18.70	4.20	$\Gamma_{CCCH}(55) + \Gamma_{OCCH}(17)$
31	874s		922	885	6.93	0.41	$\delta_{CCC}\ (38)\delta_{CCH}(10)$
32			931	894	5.26	2.25	$\Gamma_{CCCH}(70)$
33	919w	919w	950	913	49.97	4.45	$\delta_{CNH}(10) + \delta_{NNH}(11) + \Gamma_{CCNH}(12)$
34			965	927	8.80	0.33	$\Gamma_{CCCH}(76)$
35	950 ms		994	955	0.01	0.01	$\Gamma_{CCCH}(18) + \Gamma_{HCCH}(64)$
36			1032	992	13.40	23.35	$\nu_{CC}(10) + \nu_{NC}(21) + \nu_{NN}(15)$
37	1014s	1019vs	1047	1005	3.82	13.09	$\nu_{CC}(61) + \delta_{CCH}(18)$
38	1055m	1056w	1142	1097	40.98	20.22	$\nu_{CC}(32) + \nu_{NN}(23) + \delta_{CCH}(16)$
39	1119ms	1126m	1172	1126	5.46	5.73	$\nu_{CC}(19) + \nu_{NN}(14) + \delta_{CCH}(37)$
40			1183	1136	12.55	6.72	$\nu_{CC}(26) + \delta_{CCH}(57)$
41	1152s	1147m	1200	1153	26.28	7.10	$\nu_{CC}(14) + \nu_{CO}(10) + \delta_{CCH}(53)$
42	1174w	1174ms	1230	1182	211.49	34.32	$\nu_{CC}(12) + \nu_{CN}(28) + \delta_{CCH}(20)$
43	1211ms	1215ms	1256	1207	21.72	10.29	$\nu_{CC}(23) + \nu_{CN}(10) + \delta_{CCH}(28)$
44	1233m	1233m	1291	1240	13.33	8.23	$\nu_{CC}(25) + \delta_{CCH}(44)$
45	1256w	1259s	1293	1242	4.31	44.76	$\nu_{CC}(48) + \nu_{CO}(14) + \delta_{CCH}(10)$
46	1270w		1328	1276	178.03	3.22	$\nu_{CC}(21) + \nu_{CO}(16) + \delta_{COH}(14)$
47	1315m		1346	1294	3.89	8.36	$\delta_{NNH}(91)$
48			1389	1335	20.79	6.83	$\nu_{CC}(51) + \delta_{CCH}(27)$
49	1355s	1349w	1417	1361	4.51	143.92	$\nu_{CC}(67)$
50	1387m	1390vs	1436	1380	3.85	94.70	$\nu_{CC}(52) + \delta_{CCH}(10)$
51	1448w		1475	1417	70.62	27.81	$\delta_{NNH}(33) + \delta_{CNH}(23)$
52	1468w	1469ms	1501	1442	70.82	137.12	$\nu CC(27) + \delta CCH(45)$
53	1507w	1509ms	1506	1447	41.16	18.42	$\nu CC(30) + \delta CCH(28)$
54	1539w	1531ms	1555	1494	77.59	0.26	$\nu CC(46) + \delta CCH(16)$

Table 1. (*Continued*)

Mode nos.	Experimental (cm^{-1}) FT-IR	Experimental (cm^{-1}) FT-Raman	Theoretical wavenumber (cm^{-1}) B3LYP unscaled	Theoretical wavenumber (cm^{-1}) B3LYP scaled	IR_{int}	S_{act}	Characterization of normal modes with TED
55	1562m	1559m	1617	1554	16.52	20.21	νCC(46)
56		1577ms	1662	1597	24.58	11.51	δNNH(35) + δHNH(44)
57	1598m	1601m	1666	1601	45.25	13.04	νCC(57)
58	1632w	1633ms	1690	1624	196.49	118.79	νCC(65)
59	1656s		1801	1730	196.92	95.93	νOC(81)
	2707vw						Overtone/combination
	2723vw						Overtone/combination
	2854w						Overtone/combination
60		3022w	3177	3053	2.07	16.06	ν_{CH}(98)
61	3051w		3183	3058	0.55	101.56	ν_{CH}(99)
62			3195	3069	24.96	109.67	ν_{CH}(98)
63			3202	3076	4.42	4.43	ν_{CH}(98)
64			3204	3078	7.26	104.64	ν_{CH}(98)
65			3208	3082	374.42	374.42	ν_{CH}(95)
66	3286s	3285vw	3430	3296	33.54	74.59	ν_{NH}(100)
67			3463	3327	2.04	227.47	ν_{NH}(100)
68			3602	3461	8.22	122.26	ν_{NH}(99)
69	3178br		3621	3479	317.05	128.41	ν_{OH} (100)

w, weak; vw, very weak; s, strong; vs, very strong; m, medium; br sh, broad shoulder; υ, stretching; δ, in-plane bending; Γ, out-of-plane bending; IR_{int}, IR, intensity; S_{act}, Raman scattering activity.

the substitution as seen from the bond angles C11–C14–C15 and C10–C15–C14, which are calculated as 119.09° and 119.79°, respectively, by B3LYP/6-31G (d,p) and are smaller than typical hexagonal angle of 120°. The reduction in the bond angles from the normal value 120° is also evident form the increase of hexagonal angle of C4–C11–C14 and C3–C10–C15 as 122.15 and 121.39°, respectively, by B3LYP/6-31G(d,p) method. Based on above comparison, although there are some differences between the theoretical and the experimental values, the optimized structural parameters can well reproduce the experimental ones and they are basis for the discussions hereafter. The calculated geometric parameters also represent good approximations and they can be used as foundation to calculate the other parameters for the compound.

Potential energy surface scan

The potential surface scan with the B3LYP/6-31G(d,p) level of theoretical approximations was performed for title molecule as shown in Fig. 5. The dihedral angles C10–C15–O17–H18 and C14–C19–N21–N23 for hydroxyl and hydrazide group, respectively, for 3H2NAH are also the relevant coordinates for conformational flexibility within the molecules. During the calculations, all the geometrical parameters were simultaneously relaxed during the calculations while the C10–C15–O17–H18 and C14–C19–N21–N23 torsional angles were varied in steps of 10°, 20°, 30°, ..., 360°. For the C14–C19–N21–N23 rotation, the maximum energy was obtained at 100° and the minimum energy occur at 230° in the potential energy curve of energy −683.1057 and −685.1036 hatrees. For the C10–C15–O17–H18 rotation, two maximum energy positions were obtained at 60° and 260° in the potential energy curve of energy −685.0972 and −685.0971 hatrees, clearly showing that the hydroxyl group has no chance of forming the intramolecular hydrogen bonding in that angle. The minimum energy obtained is at 160°. The barrier of this rotation for 160° is −685.1090 hatrees, clearly showing that the hydroxyl group is to form the intramolecular hydrogen bonding at this position.

Vibrational assignments

Vibrational spectral assignments were performed on the recorded FT-IR and FT-Raman spectra based on the theoretically predicted wavenumbers by density functional B3LYP/6-31G(d,p) method and are collected in Table 1. None of the predicted vibrational spectra has any imaginary wavenumber, implying that the optimized geometry is located at the local lowest point on the potential energy surface. We know that *ab initio* HF and DFT potentials systematically overestimate the vibrational wavenumbers. These discrepancies are corrected either by computing anharmonic corrections explicitly or by introducing a scaled field[27] or by directly scaling the calculated wavenumbers with a proper factor.[28] Considering systematic errors with a scaling factor of 0.9608, we calibrated the vibrational wavenumbers calculated by B3LYP method. After scaling with a scaling factor, the deviation from the experiments is less than 10 cm^{-1} with a few exceptions. The title molecule belongs to C_s point group. The 69 normal modes of fundamental vibrations span the irreducible representations $47A' + 22A''$. Comparison of the wavenumbers calculated with the DFT method using 6-31G(d,p) basis set with experimental values reveals that the B3LYP method shows very good agreement with experimental observation due to inclusion of electron correlation for this method.

Journal of RAMAN SPECTROSCOPY

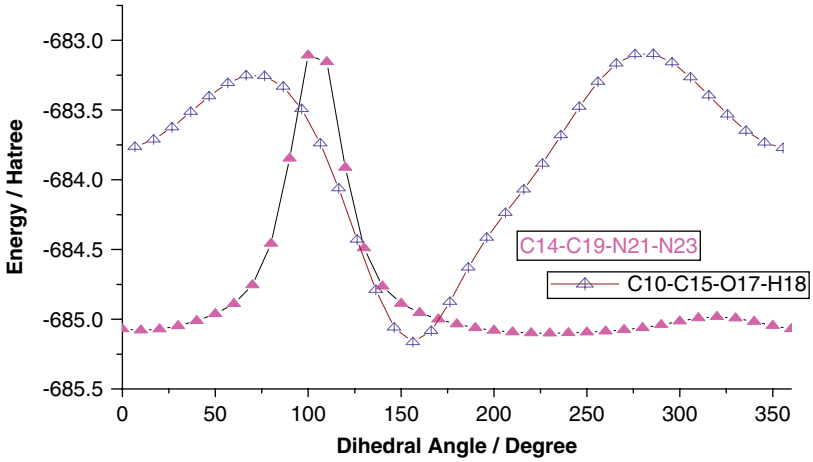

Figure 5. PES scan for dihedral angle C10–C15–O17–H18 and C14–C19–N21–N23 for 3-hydroxy-2-naphthoic acid hydrazide.

Amide group vibrations

The characteristic secondary amide bands in the stretching region, associated with N–H stretch and the overtone of N–H in-plane bending, can be observed in the IR spectrum. The major vibrational spectral effect of the intermolecular amide hydrogen bonding can be found in the N–H stretching mode. The strong band of N–H stretching extends from 3400 to 3100 cm^{-1}, with the centre of the band at 3370 cm^{-1}.[29–31] The calculated wavenumber of the above mode is 3296 cm^{-1} (mode no. 66). The strong band in the FT-IR spectrum at 3286 cm^{-1} also supports the formation of a strong N–H···O hydrogen bond. The lowering of the N–H stretching wavenumber can be attributed to the red shifting due to intermolecular N–H···O interaction. The red shifting is further enhanced by the reduction in the N–H bond order values, occurring due to donor–acceptor interaction. As expected, this mode is a pure stretching mode, and as is evident from the TED column they are almost contributing 100%. The first overtone of the N–H in-plane bending mode (~3110 cm^{-1}) falling on the N–H stretching band positions produces two bands of comparable intensities, equally displaced on either side of this wavenumber resulting from Fermi resonance with one or more N–H stretching.[29] However, our experimental measurements do not support this fact. The carbonyl stretching wavenumber has been extensively studied by infrared spectroscopy.[30] This multiple bonded group is highly polar and therefore gives rise to an intense infrared absorption band in the region 1700–1800 cm^{-1}. The carbon–oxygen double bond is formed by $p\pi - p\pi$ bonding between carbon and oxygen. Because of the different electronegativities of carbon and oxygen atoms, the bonding electrons are not equally distributed between the two atoms. The intensity of these bands can increase due to conjugation or formation of hydrogen bonds. The following two resonance forms contribute to the bonding of the carbonyl group > C═O ←->C+ - O-. The lone pair of electrons on oxygen also determines the nature of the carbonyl group.[30] In our present case, one can expect only one C═O stretching vibration corresponding to the C19═O20 mode. The experimental wavenumber observed as a strong band in the FT-IR spectrum at 1656 cm^{-1} is assigned to C═O stretching vibration, which shows moderate agreement with that obtained with the B3LYP method at 1730 cm^{-1} (mode nos.59). In this study, according to TED assignments, this mode is not contaminated with other vibrations. In keto-groups, the C═O in-plane bending vibration is found theoretically by weak peak at 378 cm^{-1} by B3LYP method. However, the experimental observation does not support this kind of vibration. The C═O out-of-plane bending vibration computed by B3LYP method at 80 cm^{-1} shows good agreement with recorded medium FT-Raman band at 98 cm^{-1}. An analysis by TED calculations shows that this vibration is coupled with ring bending mode as shown in Table 1.

C–H vibrations

Aromatic compounds commonly exhibit multiple weak bands in the region 3100–3000 cm^{-1} due to aromatic C–H stretching vibration.[31] Our title compound 3H2NAH has two aromatic ring are fused together as in Fig. 4. The 3H2NAH has six adjacent C–H moieties. The scaled vibrations, mode nos: 65–60, correspond to the stretching mode of C1–H, C2–H, C5–H, C6–H, C10–H and C11–H units. The naphthalene ring vibrations 65–60 assigned to the aromatic C–H stretch computed in the range 3082–3053 cm^{-1} by B3LYP method shows good agreement with the recorded FT-IR and FT-Raman bands at 3051–3022 cm^{-1}. All the aromatic C–H stretching bands are found to be weak, and this is due to a decrease of the dipole moment caused by reduction of negative charge on the carbon atom. This reduction occurs because of the electron withdrawal on the carbon atom by the substituent due to the decrease of inductive effect, which in turn is caused by the increase in chain length of the substitutent.[32] As expected, these six modes are pure stretching modes as it is evident from TED column, and they are almost contributing to 98%.

The naphthalene ring C–H in-plane bending vibrations lie in the region 1230–970 cm^{-1}.[33] In 3H2NAH, the medium strong bands at 1233, 1211, 1119 and 1055 cm^{-1} in the FT-IR spectrum and 1233, 1215, 1147, 1126 and 1056 in the FT-Raman spectrum are assigned to the C–H in-plane bending vibration. They show good agreement with the theoretically computed B3LYP/6-31G(d,p) method at 1240, 1207, 1153, 1136, 1126 and 1097 cm^{-1} (mode nos. 44, 43, 41–38).

The band observed at 949, 852, 792 and 740 cm^{-1} in the FT-IR spectrum and 919,793, 740 cm^{-1} in the FT-Raman are assigned to C–H out-of-plane bending vibrations for naphthalene of 3H2NAH. This also shows good agreement with theoretically scaled harmonic wavenumber values at 955, 927, 913, 894, 854, 781 and 740 cm^{-1} in B3LYP.

O–H vibrations

The OH group gives rise to three vibrations (stretching, in-plane bending and out-of-plane bending vibrations). The O–H group vibrations are likely to be the most sensitive to the environment, so they show pronounced shifts in the spectra of the hydrogen-bonded species. The hydroxyl stretching vibrations are generally[34] observed in the region around 3500 cm^{-1}. In the case of the un-substituted phenols, it has been shown that the wavenumber of O–H stretching vibration in the gas phase is at 3657 cm^{-1}.[35] Similarly in our case, a broad shouldered FT-IR band at 3178 cm^{-1} is assigned to the O–H stretching vibration. A comparison of this band with that of the computed B3LYP method predicts that there is negative deviation of 301 cm^{-1}, which reveals failure of the harmonic approximation in describing vibrations of atomic groups involved in intermolecular and intramolecular hydrogen bonds.

The O–H in-plane bending vibration for phenols, in general, lies in the region 1150–1250 cm^{-1} and is not much affected due to hydrogen bonding unlike to stretching and out-of-plane bending wavenumbers.[31] In almost all 1,2,3,5-tetrasubstituted benzene derivatives with one OH and two halogen substituents, this vibration was found in a narrow region of 1225–1252 cm^{-1}.[31] But in our study the wavenumber corresponds to the O–H in-plane bending vibration; it seems to be a little bit on the higher range by TED calculations (1276 cm^{-1}, mode no.46) and is assigned to O–H in-plane bending vibrations. This vibration mixes with C–C stretch and C–O in-plane bending vibrations as shown in Table 1.

The O–H out-of-plane deformation vibration for phenol lies in the region 290–320 cm^{-1} for free OH and in the region 517–710 cm^{-1} for associated OH.[31] In both inter-molecular and intra-molecular associations, the wavenumber is at a higher value than in free OH. The wavenumber increases with hydrogen-bond strength because of the large amount of energy required to twist the OH bond.[36] The O–H out-of-plane bending vibration computed by B3LYP/6-31G(d,p) method at 491 cm^{-1} (mode no. 16) shows good agreement with the recorded FT-IR band at 483 cm^{-1}.

NH_2 vibrations

The NH_2 group gives rise to internal modes of vibrations such as the asymmetric stretching (ν_{as}), symmetric stretching (ν_s) the symmetric planar deformation or scissoring (β_s), the anti-symmetric planar deformation or rocking (β_{as}), the symmetric non-planar deformation or wagging (ω) and the anti-symmetric non-planar deformation or torsion (τ). The molecule under investigation possesses one NH_2 group and hence one expects one asymmetric and one symmetric N–H stretching vibrations. In all the primary aromatic amines, the N–H stretching wavenumbers occur in the region 3300–3500 cm^{-1}. The antisymmetric (ν_{as}) stretching mode is calculated at the higher wavenumber 3461 cm^{-1} than the symmetric (ν_s) one at 3327 cm^{-1} by B3LYP/6-31G(d,p) method having mode nos. 68 and 67. As seen in Table 1 (mode nos. 68 and 67), the N–H stretching vibrations are pure, and as is evident from the TED column they are almost contributing to 100%. However, the experimental observation shows that no such band exists in this region, because of the overlapping of the O–H and N–H stretching vibrations.

The internal deformation vibration known as NH_2 scissoring wavenumber, found as a medium band at 1577 cm^{-1} in the FT-Raman spectrum, is well within the range by the B3LYP computed wavenumber at 1597 cm^{-1} (mode nos. 56). The NH_2 wagging mode computed at 822 cm^{-1} (mode no.28) by B3LYP/6-31G(d,p) shows good agreement with literature data. The N–NH_2 in-plane and out-of-plane bending vibrations computed by the B3LYP method show good agreement with the recorded spectrum. The NH_2 rocking and torsional predicted modes and experimental observations also show consistent agreement, as shown in Table 1.

Ring vibrations

Several ring vibrations are affected by the substitution to the aromatic ring of naphthalene. The naphthalene ring vibrations are found to make a major contribution in the IR and Raman spectra of the sample. The naphthalene ring stretching vibrations usually occur in the region 1580–1300 cm^{-1}.[33,37] For aromatic six-membered rings, e.g. benzene and pyridines, there are two or three bands in this region due to skeletal vibrations, the strongest usually being at about 1500 cm^{-1}. In the case where the ring is conjugated further, a band at about 1580 cm^{-1} is also observed. For substituted benzenes with identical atoms or groups on all para-pairs of ring carbon atoms, the vibrations causing the band at 1625–1590 cm^{-1} are infrared inactive due to symmetry considerations, as the compound has a centre of symmetry at the ring center. If the groups on a para-pair of carbon atoms are different, then there is no centre of symmetry and the vibrations are infrared active.[30] Chithambarathanu *et al*.[38] have observed the FT-IR bands at 1574, 1498 and 1468 cm^{-1} in 1,3,5-triphenyl-4,5-dihydropyrazole. Neville and Shurvell[39] have identified the IR bands at 1470, 1484, 1561, 1575 and 1590 cm^{-1} in diazepam and closely related compounds of benzodiazepines due to aromatic C–C stretching vibrations. Based on the above conclusion, in the present study the C–C stretching vibration due to conjugation of two aromatic ring observed in FT-IR bands at 1632, 1539, 1507, 1387, 1355, 1256 cm^{-1} and at 1633, 1601, 1559, 1531, 1509, 1469, 1390, 1349, 1259 cm^{-1} in FT-Raman spectrum are assigned to C–C stretching vibration.

In a few of these modes, the contribution of NH_2 scissoring vibrations are also present. This kind of mixing of modes is a consequence of the lowering of symmetry and it has been observed in mono-substituted benzenes, nitrobenzenes, phenol, benzaldehyde, azobenzenes, naphthalene and coumarin.[39] In addition, there are several C–C–C in-plane and out-of -plane bending vibrations of the naphthalene ring carbons. The C–C–C in plane and out-of-plane bending vibration is in agreement with both experimental and theoretical spectral data. Small changes in wavenumber observed for these modes are due to the change in force constants/reduced mass ratio resulting mainly from the extent of mixing between ring and substituent groups.

Absorption spectra

On the basis of a fully optimized ground-state structure, the TD-DFT//B3LYP/6-31G(d,p) calculations have been used to determine the low-lying excited states of 3H2NAH. The calculated results involving the vertical excitation energies, oscillator strength (*f*) and wavelength are carried out and compared with measured experimental wavelength. Typically, according to the Frank–Condon principle, the maximum absorption peak (λ_{max}) corresponds in a UV-visible spectrum to vertical excitation. The D-DFT//B3LYP/6-31G(d,p) calculation predicts one intense electronic transition at (225.4 nm) with an oscillator strength $f = 0.518$, in good agreement with the measured experimental data ($\lambda_{exp} = 234$ nm) as shown in Fig. 3. This electronic absorption corresponds to the

Journal of RAMAN SPECTROSCOPY

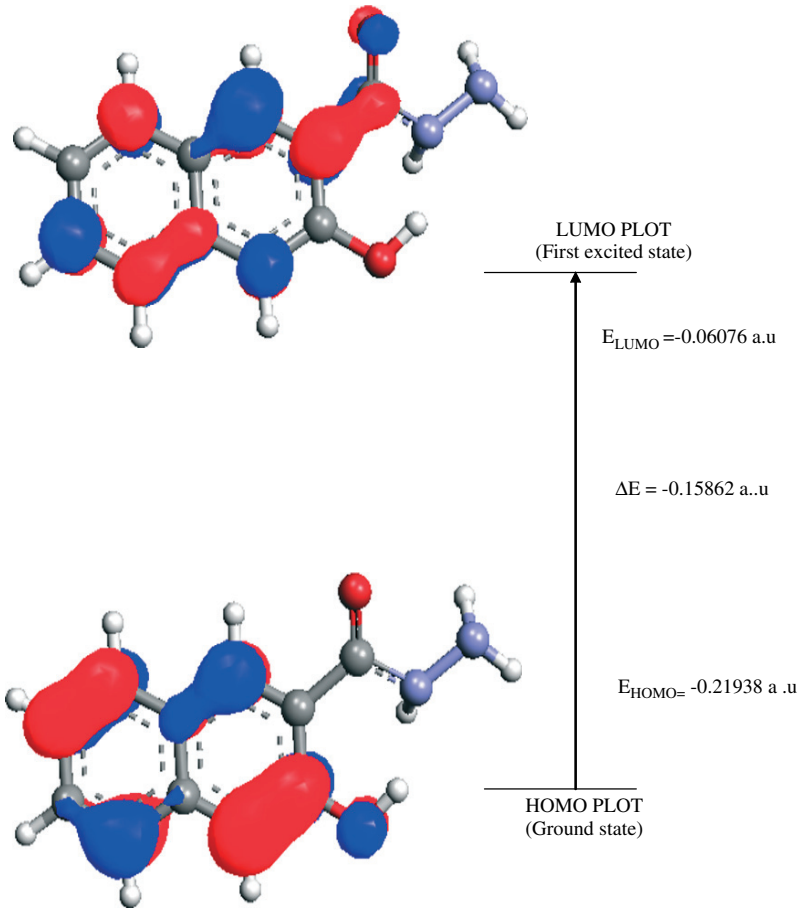

Figure 6. The atomic orbital compositions of the frontier molecular orbital for 3-hydroxy-2-naphthoic acid hydrazide.

transition from the ground to the first excited state and is mainly described by one electron excitation from the highest occupied molecular orbital (HOMO) to the lowest unoccupied molecular orbital (LUMO).

The HOMO is located over naphthalene and OH group, and the HOMO → LUMO transition implies an electron density transfer to the hydrazide group from the naphthalene ring and hydroxyl group. Moreover, these orbitals significantly overlap in their position for 3H2NAH. The atomic orbital compositions of the frontier molecular orbital are sketched in Fig. 6.

The HOMO–LUMO energy gap of 3H2NAH was calculated at the B3LYP/6-31(d,p) and HF/6-31G(d,p) level and is shown in Table S1 (Supporting Information), which reveals that the energy gap reflects the chemical activity of the molecule. The LUMO as an electron acceptor represents the ability to obtain an electron, and HOMO represents the ability to donate an electron.

The calculated self-consistent field (SCF) energy of 3H2NAH is −685.146 a.u. Moreover, a lower HOMO–LUMO energy gap explains the fact that eventual charge transfer interaction is taking place within the molecule.

Conclusions

The NIR-FT-Raman and FT-IR spectral studies of 3H2NAH were carried out for the first time. The difference between the observed and scaled wavenumber values of most of the fundamentals is very small. However, the difference between the observed and scaled wavenumber values of the OH and amide group fundamentals is very large, due to the presence of the intermolecular and intramolecular hydrogen bonds in the solid state, which must be reflected in the IR spectra. Therefore, the assignments made at DFT level of theory with only reasonable deviations from the experimental values seem to be correct. The theoretically constructed FT-IR and FT-Raman spectra exactly coincide with experimentally observed FT-IR and FT-Raman spectra. Furthermore, the thermodynamic, nonlinear optical, first-order hyperpolarizabilities and total dipole moment properties of the compound have been calculated in order to get insight into the compound. The UV spectrum was measured in ethanol solution. We hope the results will be of assistance in the quest of the experimental and theoretical evidence for the title molecule in reaction intermediates, nonlinear optical and photoelectric materials.

Supporting information

Supporting information may be found in the online version of this article.

References

[1] S. Khasnobis, E. E. Vincent, D. Chatterjee, *Expert Opin. Ther. Targets* **2002**, *6*, 21.
[2] R. J. O'Brien, P. P. Nunn, *Am. J. Respir. Crit. Care Med.* **2001**, *163*, 1055.
[3] A. Kochi, *Tubercle* **1991**, *72*, 1.

[4] DOTS-plus: preliminary results and emerging issues, *Proceedings of the Meeting of the Stop TB Working Group on DOTS-Plus for MDR-TB*, Tallinn, Estonia, 10–12 April 2002, **2002**, http://www.who.int/gtb/publications/dotsplus/TB-**2002**-307.pdf.
[5] C. D. Hamilton, *Curr. Infect. Dis. Rep.* **1999**, *1*, 80.
[6] G. B. Migliori, M. Ambrosetti, L. Fattorini, V. Penati, P. Vaccarino, G. Besozzi, L. Ortona, C. Saltini, G. Orefici, M. L. Moro, E. Lona, A. Cassone, *Int. J. Tuberc. Lung Dis.* **2000**, *4*, 940.
[7] D. W. Fitzgerald, M. M. Morse, J. W. Pape, W. D. Johnson, *Clin. Infect. Dis.* **2000**, *31*, 1495.
[8] F. Stieber, U. Grether, A. Giannis, R. Mazitschek, H. Waldmann, N. Soric, *Chem. Eur. J.* **2003**, *9*, 3282.
[9] P. Melnyk, V. Leroux, C. Sergheraert, P. Grellier, *Bioorg. Med. Chem. Lett.* **2006**, *16*, 31.
[10] S. G. Kucukguzel, A. Mazi, F. Sahin, S. Ozturk, J. Stables, *Eur. J. Med. Chem.* **2003**, *38*, 1005.
[11] M. Mashima, *Bull. Chem. Soc. Jpn.* **1962**, *35*, 1885.
[12] P. J. V. Koningsbruggen, E. Müller, J. G. Haasnoot, J. Reedijk, *Inorg. Chim. Acta* **1993**, *208*, 37.
[13] S. Samdal, H. Møllendal, *J. Phys. Chem.* **2003**, *107A*, 8845.
[14] V. P. Sinditskii, M. D. Dutov, A. E. Fogel'zang, *Chem. Heterocycl. Comp.* **1991**, *27*, 72.
[15] H. N. Dogan, S. Rollas, H. Erdeniz, *Il Farmaco* **1998**, *53*, 46247.
[16] D. Sajan, J. Binoy, B. Pradeep, K. Venkatakrishnan, V. B. Kartha, I. H. Joe, V. S. Jayakumar, *Spectrochim. Acta* **2004**, *60A*, 173.
[17] J. P. Abraham, I. H. Joe, V. George, O. F. Nielson, V. S. Jayakumar, *Spectrochim. Acta* **2003**, *59A*, 193.
[18] J. Binoy, J. P. Abraham, I. H. Joe, V. S. Jayakumar, J. Aubard, O. F. Nielson, *J. Raman Spectrosc.* **2005**, *36*, 63.
[19] Gaussian Inc., *Gaussion 03 Program*, Gaussian Inc.: Wallingford, **2004**.
[20] H. B. Schlegel, *J. Comput. Chem.* **1982**, *3*, 214.
[21] J. Baker, A. A. Jarzccki, P. Pulay, *J. Phys. Chem.* **1998**, *102 A*, 1412.
[22] P. Pulay, G. Fogarasi, G. Pongor, J.E. Boggs, A. Vargha, *J.Am.Chem.Soc.* **1983**, *105*, 7037.
[23] G. Keresztury, S. Holly, J. Varga, G. Besenyei, A. Y. Wang, J. R. Durig, *Spectrochim. Acta* **1993**, *49A*, 2007.
[24] G. Keresztury, J. M. Chalmers, P. R. Griffith (Eds), Raman spectroscopy: theory, *Hand Book of Vibrational Spectroscopy*, vol. 1, John Wiley & Sons Ltd: New York, **2002**.
[25] D. A. Kleinman, *Phys. Rev.* **1962**, *126*, 1977.
[26] S. Naveen, S. M. Anandalwar, J. S. Prasad, I. Jathi, K. L. Godwin, S. K. Balladka, K. K. Vijayaraj, *Anal. Sci.* **2006**, *22*, 159.
[27] P. Pulay, G. Fogarasi, G. Pongor, J. E. Boggs, A. Vargha, *J. Am. Chem. Soc.* **1983**, *105*, 7037.
[28] A. P. Scott, L. Radom, *J. Phys. Chem.* **1996**, *100*, 16502.
[29] N. B. Colthup, L. H. Daly, S. E. Wiberley, *Introduction to Infrared and Raman Spectroscopy*, Academic Press: New York, **1990**.
[30] G. Socrates, *Infrared Characteristic Group Frequencies*, Wiley, Interscience Publication: New York, **1980**.
[31] G. Varsanyi, *Assignments for Vibrational Spectra of Seven Hundred Benzene Derivatives*, vols. 1 and 2, Academiai Kiado: Budapest, **1973**.
[32] N. Sundaraganesan, H. Saleem, S. Mohan, *Spectrochim Acta* **2003**, *59A*, 2511.
[33] A. J. Barnes, *Spectrochim Acta* **1985**, *41 A*, 629.
[34] D. Sajan, I. Hubert Joe, V. S. Jayakumar, J. Zaleski, *J. Mol. Struct.* **2006**, *785*, 43.
[35] D. Michalska, D. C. Bienko, A. J. A. Bienko, Z. Latajka, *J. Phys. Chem.* **1996**, *100*, 1186.
[36] I. D. Sadekov, *Russ. Chem. Rev.* **1970**, *39*, 179.
[37] C. Sourisseau, P. Maraval, *J. Raman Spectrosc.* **1994**, *25*, 477.
[38] T. Chithambarathanu, V. Umayourbaghan, V. Krishnakumar, *Indian J. Pure Appl. Phys.* **2003**, *41*, 844.
[39] G. A. Neville, H. F. Shurvell, *J. Raman Spectrosc.* **1990**, *21*, 9.